Convergence of TCR and cytokine signaling leads to FOXO3a phosphorylation and drives the survival of CD4+ central memory T cells

Catherine Riou,[1,2,3] Bader Yassine-Diab,[1] Julien Van grevenynghe,[1,3] Roland Somogyi,[5] Larry D. Greller,[5] Dominic Gagnon,[1] Sylvain Gimmig,[1] Peter Wilkinson,[1] Yu Shi,[1] Mark J. Cameron,[6] Roberto Campos-Gonzalez,[7] Robert S. Balderas,[7] David Kelvin,[6] Rafick-Pierre Sekaly,[1,2,3,4] and Elias K. Haddad[1,2,3,4]

[1]Laboratoire d'Immunologie, Centre de Recherche, Hôpital Saint-Luc du Centre Hospitalier de l'Université de Montréal (CHUM), Montréal, Québec H2X 1P1, Canada
[2]Laboratoire d'Immunologie, Département de Microbiologie et d'Immunologie, Université de Montréal, Montréal, Québec H3T 1J4, Canada
[3]Institut national de la santé et de la recherche médicale U743, Centre de Recherche, CHUM, Université de Montréal, Montréal, Québec H2X 1P1, Canada
[4]Department of Microbiology and Immunology, McGill University, Montréal, Québec H3A 2B4, Canada
[5]Biosystemix, Ltd., Sydenham, Ontario K0H 2T0, Canada
[6]Toronto General Research Institute, University Health Network, Toronto, Ontario M5G 2M9, Canada
[7]BD Biosciences, San Diego, CA 92121

The molecular events involved in the establishment and maintenance of CD4+ central memory and effector memory T cells (T_{CM} and T_{EM}, respectively) are poorly understood. In this study, we demonstrate that ex vivo isolated T_{CM} are more resistant to both spontaneous and Fas-induced apoptosis than T_{EM} and have an increased capacity to proliferate and persist in vitro. Using global gene expression profiling, single cell proteomics, and functional assays, we show that the survival of CD4+ T_{CM} depends, at least in part, on the activation and phosphorylation of signal transducer and activator of transcription 5a (STAT5a) and forkhead box O3a (FOXO3a). T_{CM} showed a significant increase in the levels of phosphorylation of STAT5a compared with T_{EM} in response to both IL-2 ($P < 0.04$) and IL-7 ($P < 0.002$); the latter is well known for its capacity to enhance T cell survival. Moreover, ex vivo T_{CM} express higher levels of the transcriptionally inactive phosphorylated forms of FOXO3a and concomitantly lower levels of the proapoptotic FOXO3a target, Bim. Experiments aimed at blocking FOXO3a phosphorylation confirmed the role of this phosphoprotein in protecting T_{CM} from apoptosis. Our results provide, for the first time in humans, an insight into molecular mechanisms that could be responsible for the longevity and persistence of CD4+ T_{CM}.

CORRESPONDENCE
Rafick-Pierre Sekaly:
rafick-pierre.sekaly@umontreal.ca

Abbreviations used: ANOVA, analysis of variance; CCR, CC chemokine receptor; FOXO3a, forkhead box O3a; HRP, horseradish peroxidase; IKK, IκB kinase; mDC, mature DC; MFI, mean fluorescence intensity; PCA, principal component analysis; SEA, staphylococcal enterotoxin superantigen; T_{CM}, T_{EM}, and T_{TM}, central memory, effector memory, and transitory memory T cell(s), respectively.

The generation and maintenance of memory T cells is central to the development of protective immunity, as characterized by a rapid and vigorous response after the encounter with a given pathogen or antigen (1, 2). Despite the complexity of the memory T cell populations, recent studies in both mice and humans indicate that the memory T cell pool is composed of two main compartments, central memory and effector memory T cells (T_{CM} and T_{EM}, respectively), which are characterized by distinct homing capacities and effector functions (3, 4). Through their expression of CC chemokine receptor (CCR) 7 and CD62L, T_{CM} preferentially home to T cell areas of secondary lymphoid organs and display few immediate effector functions; however, they readily proliferate and differentiate to effector cells in response to antigenic stimulation. T_{EM} that have lost the constitutive expression of CCR7

The online version of this article contains supplemental material.

The Journal of Experimental Medicine

express tissue-homing receptors associated with inflammation and more readily display effector functions. The current model proposes that upon reinfection, T_{EM} rapidly constrain pathogen invasion in inflamed peripheral tissues, whereas T_{CM} are rapidly activated by DCs in secondary lymphoid organs and generate successive waves of effectors able to completely eliminate the pathogen (2).

Experiments performed in mouse models suggest that T_{CM} have a better capacity to reconstitute the memory T cell pool and to mediate protective immunity than T_{EM} because of their greater capacity to proliferate and persist in vivo (5, 6). Studies in primate models show that induction of central memory $CD4^+$ T cells after SIV challenge correlates with prolonged survival (7), thereby highlighting the importance of gaining a better understanding of the mechanisms underlying T_{CM} induction and persistence for successful vaccine development. The molecular mechanisms underlying the persistence of these cell subsets are still unknown, and it remains unclear whether T_{CM} and T_{EM} use the same mechanisms to persist in the host. The long-term maintenance of memory T cells relies on the survival of individual cells and their level of homeostatic cell division to compensate for their gradual attrition through apoptosis (2, 8). Using in vivo labeling with deuterated glucose to measure the turnover of distinct subsets of $CD4^+$ T cells in healthy humans, Macallan et al. have shown that T_{EM} have a more rapid turnover than T_{CM}, suggesting that T_{EM} are being replaced at a faster rate than T_{CM} (9). These different turnover rates might be attributed to intrinsic differences in their susceptibility to apoptosis, although this has never been directly addressed.

The nature of the signals that ensure the persistence of T_{CM} is under intense investigation. Results obtained in mouse

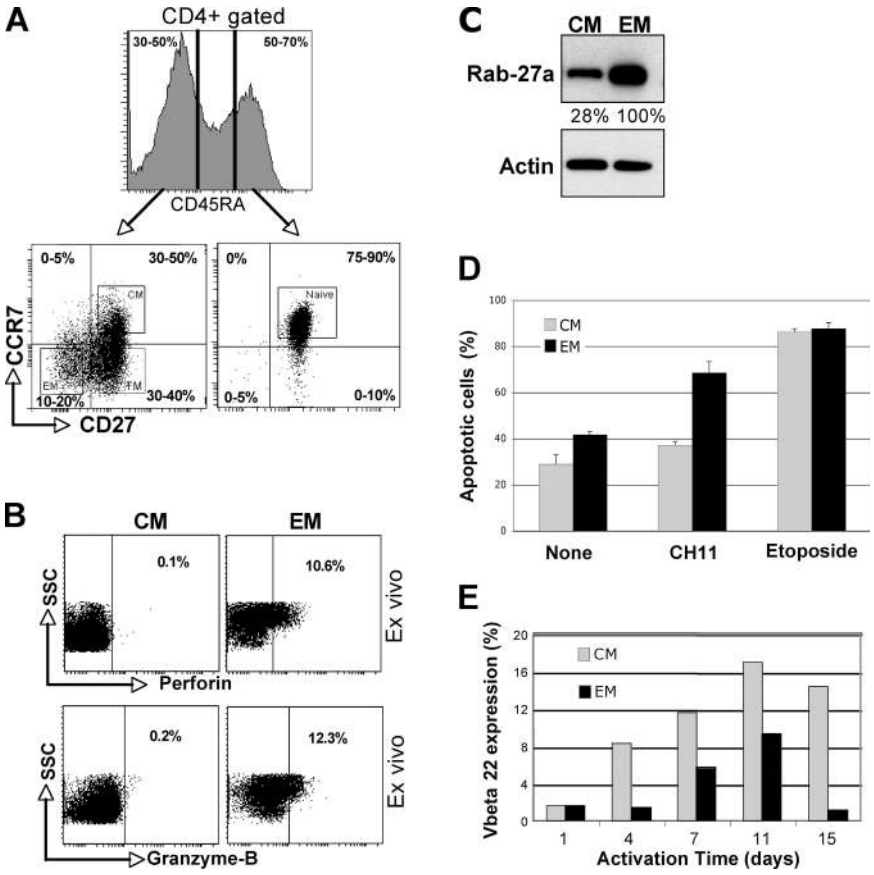

Figure 1. Functional and phenotypical characterization of $CD4^+$ T_{CM} and T_{EM}. (A) CD45RA, CD27, and CCR7 labeling profile and gating strategy for naive, T_{CM}, and T_{EM}. Percentages obtained for each population are indicated. The purity of sorted cells was consistently >95%. (B) Perforin and Gr-B expression in ex vivo T_{CM} and T_{EM} subsets. Perforin and Gr-B expression were assayed by intracellular staining. The percentages of T_{CM} and T_{EM} expressing perforin and Gr-B are indicated in each quadrant. SSC, side scatter. (C) Rab-27a protein levels in ex vivo sorted T_{CM} and T_{EM} subsets. Similar results were obtained in three independent experiments. (D) Susceptibility of T_{CM} and T_{EM} to Fas-induced apoptosis. T_{CM} and T_{EM} were sorted by flow cytometry and treated with 1.25 μg/ml of the anti-Fas antibody CH11 or 100 μg/ml etoposide for 24 h. The percentage of apoptotic cells was assessed by flow cytometry using Annexin V labeling. The results are depicted as a percentage of apoptotic cells ± SD of three independent experiments. (E) Proliferation and persistence of purified T_{CM} and T_{EM}. Sorted T_{CM} and T_{EM} were co-cultured with mDCs in the presence of superantigen (SEA) for 15 d. After 1–15 d, the proportion of proliferating cells was assessed by staining of anti-TCRVβ22, as Vβ22 is known to be a highly SEA-reactive Vβ. Results are represented as the percentage of Vβ22-positive cells.

models have suggested that signaling through TCR and γ chain cytokine receptors is required for long-term survival of memory T cells (10–13). For example, memory CD4 cells persisted for extended periods upon adoptive transfer into intact or lymphopenic recipients but not in IL-$7^{-/-}$ mice (11). Moreover, Kassiotis et al. have demonstrated that the homeostatic expansion capacity of both $CD4^+$ naive and memory cells is dependent on the expression levels of TCR and CD5, a negative regulator of TCR signaling (13). It is possible that T_{CM} and T_{EM} respond distinctively to these signals, thereby influencing their long-term maintenance. In this study, we have used gene and protein expression profiling and functional assays of human $CD4^+$ T_{EM} and T_{CM} to identify the mechanisms underlying their maintenance. Our results provide a molecular basis for the capacity of $CD4^+$ T_{CM} to resist apoptosis and to persist in a stable manner in the host, thereby conferring long-term protective immunity against reinfection.

RESULTS

Functional and phenotypic characterization of $CD4^+$ T_{CM} and T_{EM}

Memory T cell subsets were sorted by flow cytometry from whole PBMCs isolated from 13 healthy donors based on CD45RA, CD27, and CCR7 expression. Naive cells are characterized as $CD45RA^+$, $CD27^+$, and $CCR7^+$; T_{CM} have the phenotypes $CD45RA^-$, $CD27^+$, and $CCR7^+$; T_{EM} are defined by the lack of expression of these three markers ($CD45RA^-$, $CD27^-$, and $CCR7^-$) (Fig. 1 A) (14); and transitory memory T cells (T_{TM}) are characterized as $CD45RA^-$, $CD27^+$, and $CCR7^-$ (T_{TM}; Fig. 1 A). All T_{CM} (>95%) expressed CD28, CD62L, and CD95. T_{EM} were also homogeneously $CD28^+$ and $CD95^+$, albeit only 30–40% expressed CD62L (unpublished data). As expected, the ex vivo sorted T_{EM} subpopulation expressed the effector molecules granzyme B and perforin, whereas these two molecules were undetectable in T_{CM} (Fig. 1 B). T_{EM} also showed higher

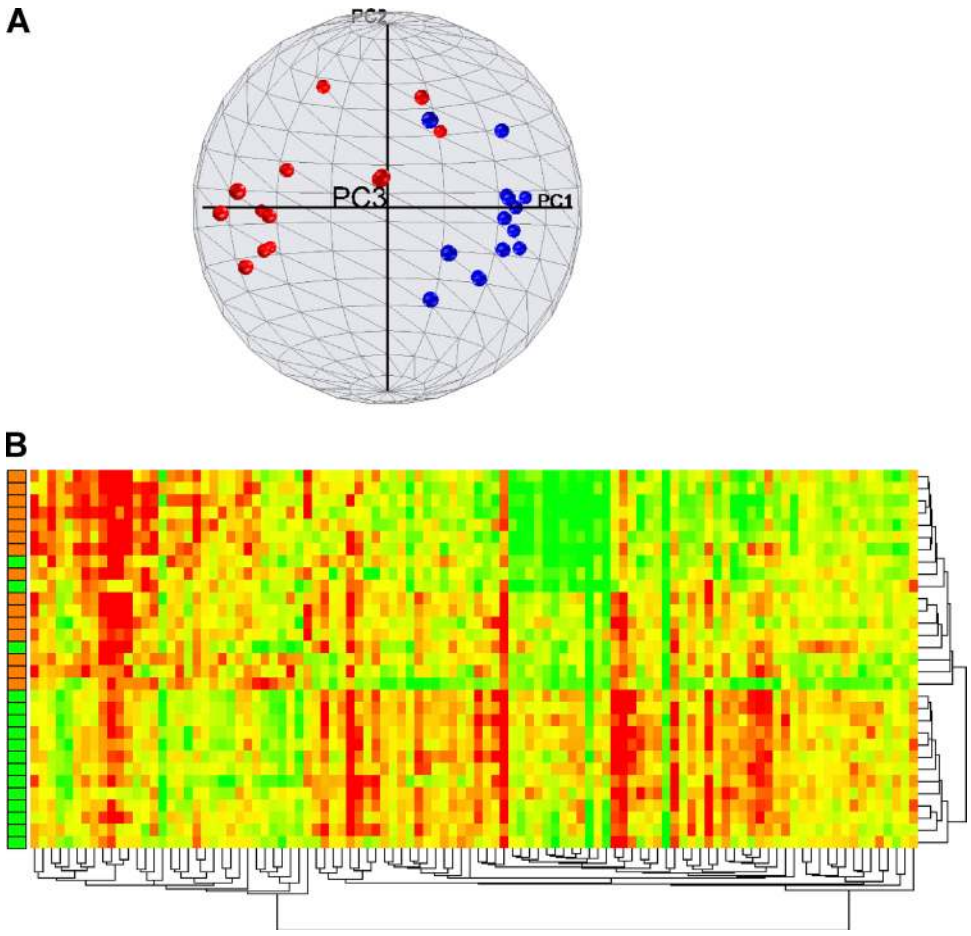

Figure 2. Gene expression array analysis of ex vivo $CD4^+$ T_{CM} and T_{EM}. (A) PCA. T_{CM} (blue) separate well from T_{EM} (red) in this three-dimensional projection of the first three principal components. (B) Two-way hierarchical clustering of $CD4^+$ T_{CM} and T_{EM} expression profiles. The far left column represents sample labels, with T_{CM} donors shown as green squares, and T_{EM} donors shown as orange squares. Each additional column represents a different gene; green indicates lower than median expression (down-regulation) and red indicates higher than median expression (up-regulation). The results of the two-dimensional hierarchical clustering of genes and samples (Pearson correlation similarity measure) are shown as horizontal and vertical dendrograms.

(threefold) expression levels of Rab27a, a molecule involved in degranulation and effector function (15), than T_{CM} (Fig. 1 C). Collectively, these results show that T_{EM} are functionally and phenotypically more differentiated than T_{CM}.

CD4$^+$ T_{CM} are resistant to Fas-induced apoptosis and show enhanced proliferation capacity after stimulation with mature DCs (mDCs)

T_{CM} are long lived and should thus be resistant to cell death signals. We therefore determined their sensitivity to apoptosis as compared with the shorter-lived T_{EM}. Sorted T_{CM} and T_{EM} were cultured in the presence or absence of anti-Fas antibody or etoposide for 24 h ($n = 3$). Annexin V labeling showed a significant difference ($P \leq 0.007$) in the capacity of T_{CM} to resist Fas-mediated apoptosis as compared with T_{EM} (Fig. 1 D). Of note, T_{CM} are less prone to undergo spontaneous apoptosis (i.e., without any apoptotic inducers; $P \leq 0.02$) than the T_{EM} subset (Fig. 1 D). Moreover, in response to etoposide, used as a nonspecific apoptotic inducer, both T_{CM} and T_{EM} present similar sensitivity to apoptosis, thereby confirming that the apoptotic machinery is intact in both cell types. We also determined the capacity of purified T_{CM} and T_{EM} to proliferate and persist in a 15-d culture assay after stimulation with staphylococcal enterotoxin superantigen (SEA)–pulsed mDCs. Proliferation was determined by quantifying the expansion of the SEA-responsive TCRVβ22$^+$ T cells. T_{CM} present a better expansion potential and can persist longer than T_{EM}, as demonstrated by a 10-fold increase in the absolute number of SEA-responsive TCRVβ22$^+$ T cells in a 15-d culture period (Fig. 1 E). Similar data were also generated using carboxyfluorescein diacetate succinimidyl ester, whereby T_{CM} undergo several more rounds of proliferation when compared with T_{EM} (unpublished data). Collectively, these results demonstrate that CD4$^+$ T_{CM} and T_{EM} subsets exhibit different capacities to proliferate, persist, and undergo both spontaneous and Fas-induced apoptosis. These observations

Table I. Differential expression of apoptosis-related genes in CD4$^+$ T_{CM} and T_{EM}

Gene	Name	Accession number	p-value[a]	AVG FC[b]	GO annotation
MAL	T cell differentiation protein	AK096093	0.02016	2.68	Proapoptotic
NGFRAP1	TNFRSF16-associated protein 1	CR593909	0.01641	2.55	Apoptosis
TNFRSF7	TNF receptor 7	CR624829	0.05641	2.37	Antiapoptotic
RELA	Transcription factor NF-κB3	BC033522	0.01149	2.17	Antiapoptotic
TOSO	Fas apoptotic inhibitory molecule 3	NM_005449	0.07717	2.15	Antiapoptotic
PIM2	Pim-2 oncogene	NM_006875	0.00954	1.93	Antiapoptotic
STAT5a	Signal transducer and activator of transcription	NM_003152	0.00543	1.72	Antiapoptotic
TNFRSF8	TNF receptor 8	AA147604	0.00511	1.51	Apoptosis
NOTCH3	In multiple clusters		0.01807	1.39	Antiapoptotic
TNF-a	TNF member 2	BC028148	0.00372	1.38	Proapoptotic
E2F1	E2F transcription factor 1	BC050369	0.03707	1.38	Proapoptotic
TNFSF7	TNF ligand 7	BM464627	0.00271	1.37	Antiapoptotic
BIRC6	Apollon	NM_016252	0.05593	1.34	Antiapoptotic
NGFR	NGF receptor 16	AK125088	0.00767	1.34	Proapoptotic
CASP3	**Caspase 3**	**NM_004346**	**0.05753**	**−1.33**	**Proapoptotic**
TNFRSF1B	**TNF receptor 1B**	**BC052977**	**0.02560**	**−1.39**	**Pro- or antiapoptotic**
CASP8	**Caspase 8**	**NM_033357**	**0.07165**	**−1.44**	**Proapoptotic**
YARS	**Tyrosyl-tRNA synthetase**	**AK125213**	**0.14050**	**−1.46**	**Proapoptotic**
TGIF	**TGF-β–induced factor**	**NM_170695**	**0.07018**	**−1.59**	**Proapoptotic**
IGFBP1	**IGF factor binding protein 1**	**NM_004943**	**0.01336**	**−1.65**	**FOXO3a target**
CLU	**Clusterin**	**NM_203339**	**0.03113**	**−1.84**	**Proapoptotic**
GZMB	**Granzyme B**	**BQ052893**	**0.00231**	**−1.93**	**Proapoptotic**
LGALS3	**Galectin 3**	**AB209391**	**0.13870**	**−2.04**	**Proapoptotic**
LGALS1	**Galectin 1**	**BF570935**	**0.06611**	**−2.49**	**Proapoptotic**

Significant genes were selected using an ANOVA *t* test ($P < 0.05$ or a fold change >1.7) and associated with an "apoptosis" GO annotation. Each gene on the arrays was spotted in duplicate to avoid false positive signals and to ensure the reproducibility of the data obtained. The fold change values were obtained from the average value of 13 independent hybridizations (AVG FC). The genes upregulated in T_{EM} are bolded. A complete list of 270 genes is available in Table S1.

[a]The p-values were determined by ANOVA, based on an F-test.

[b]Fold change values were calculated from the average value of 13 independent hybridizations by subtracting the mean expression of the log2 ratio obtained in T_{CM} from the log2 ratio obtained in T_{EM}. That value was then converted into fold change.

led us to investigate the cell survival pathways responsible for that resistance to cell death in T_{CM} and to characterize the differences in these pathways between T_{CM} and T_{EM}.

Gene array analysis of T_{CM} and T_{EM} showed differences in gene expression associated with survival pathways

Sorted T_{CM} and T_{EM} were hybridized on two different chips: the custom immune array (~3,000 unique transcripts) and a standardized 19K array (~10,000 unique transcripts). The first level of analysis was performed by submitting 26 samples (13 replicates per class) to unsupervised cluster analysis using principal component analysis (PCA). PCA enables the discrimination and visual clustering of two or more classes, where objects with similar patterns of gene expression are placed next to each other. As shown in Fig. 2 A, T_{CM} and T_{EM} visually segregate on a PCA plot. The distance separating T_{CM} from T_{EM} reflects differences in overall gene expression between the two subsets. These differences were observed in most samples (10 out of 13 T_{CM} clustered together with three outliers). Two-way hierarchical clustering of T_{CM} and T_{EM} (Fig. 2 B) further demonstrated that T_{CM} and T_{EM} subsets group apart and that the gene expression signature of T_{CM} is considerably different than that of T_{EM}.

Using single gene searches, we identified the genes that distinguished T_{CM} from T_{EM}. Genes selected using analysis of variance (ANOVA), where $P < 0.05$ or a fold change >1.7 were considered significant. We identified >270 significant genes that distinguished both subsets. Within the selected genes, 6% were related to apoptosis, 9% to cell cycle, and 7% to signaling. These genes also encompassed biological functions, including (a) homing and adhesion, (b) gene expression regulation, (c) immune response, and (d) transport. The complete list of genes can be found in Table S1 (available at http://www.jem.org/cgi/content/full/jem.20061681/DC1). Apoptosis-related genes displaying a different expression profile when comparing T_{CM} with T_{EM} are listed in Table I. T_{CM} expressed higher levels of *TOSO*, *CD27*, *STAT5a*, *PIM-2*, *RelA*, and *Birc6* (*Bruce*) mRNA, all belonging to distinct antiapoptotic pathways (16–20), than their T_{EM} counterparts. In contrast, T_{EM} showed higher levels of expression of genes involved in the induction of apoptosis, including *caspase-8* and *caspase-10*, as well as several proteins endowed with a proapoptotic function, such as *galectin-1* and *galectin-3* (21), *clusterin* (22), *YARS* (23), and *TGIF*, a TGFβ-targeted gene (24). This expression profile suggested that T_{EM} contain an active proapoptotic machinery, thereby explaining their enhanced susceptibility to cell death (Fig. 1 D). On the other hand, several genes that promote cell survival were selectively expressed at high levels in T_{CM}, rendering them more resistant to apoptosis. Of note, T_{TM} ($CD45RA^-$, $CD27^+$, and $CCR7^-$) display an intermediary phenotype between T_{CM} and T_{EM}. Indeed, their gene expression profiles are very much comparable to T_{EM} for certain genes (including *CD62L*, *TOSO*, and *PIM2*) and to T_{CM} for other genes such as *Bim*, *FasL*, or *IFN-γ* (Fig. S1).

In the next set of experiments, we validated and detailed the gene array data by performing real-time RT-PCR on the same donor samples (Table II). The results showed a significant increase in the forkhead box O3a (FOXO3a) transcriptional target proapoptotic genes, including *Bim* (25), *FasL* (26), and genes involved in cell cycle regulation, including *GADD45a* (27) and *p130*, a member of the retinoblastoma family (28) in the T_{EM} subset. Furthermore, the RT-PCR data confirmed the up-regulation of the survival gene *CD27* and the antiapoptotic *PIM-2* kinase, with the latter being regulated by the STAT5a cascade in T_{CM} (29). These results validated our gene array data and further suggested the involvement of STAT5a and FOXO3a signaling pathways in mediating the survival of T_{CM}.

STAT5a signaling pathway is functionally up-regulated in T_{CM}

STAT5a is a downstream effector of γc cytokine receptors (30). We observed differential expressions of PIM-1 and PIM-2, two transcriptional targets of STAT5a in the ex vivo T_{CM} subset. Indeed, T_{CM} showed twofold higher expression of both PIM-1 and PIM-2 than T_{EM} ($n = 3$; Fig. 3 A). Because of the importance of the STAT5a pathway in the

Table II. Real-time RT-PCR of differential gene expressions in T_{CM} and T_{EM}

Gene	Fold change T_{CM}/T_{EM}[a]	Fold change T_{EM}/T_{CM}[a]	Function	Accession number
CD27	11.2		Antiapoptotic	NM_001242
PIM-2	2.2		Antiapoptotic	NM_006875
Bim		**3.1**	**Proapoptotic**	**NM_006538**
FasL		**7.3**	**Proapoptotic**	**NM_000639**
GADD45a		**2.5**	**Cell cycle**	**NM_001924**
P130 RBL2		**1.4**	**Cell cycle**	**NM_005611**
P27Kip		**3.2**	**Cell cycle**	**NM_004064**
LKLF	4.1		Quiescence	NM_016270
DUSP6		**5.9**	**AKT inhibitor**	**NM_001946**

Total mRNA was isolated from T_{CM} and T_{EM} and analyzed by quantitative RT-PCR using a low density array. The bolded genes are up-regulated in T_{EM}, whereas the other genes are up-regulated in T_{CM}. Fold changes represent the changes in transcript level in T_{EM} compared to T_{CM} for two donors.
[a]Fold change values were calculated from the average value of two independent experiments using log2 ratio values converted to fold change.

regulation of T cell survival (30), we evaluated the ability of IL-2 and IL-7 to trigger the STAT5a signaling pathway in $CD4^+$ T cell memory subsets. The phosphorylated form of STAT5a (Y694; pSTAT5a) was quantified by flow cytometry. Basal pSTAT5a levels were similar in T_{CM} and T_{EM} (Fig. 3 B). All T_{CM} and T_{EM} up-regulated pSTAT5a in response to a brief IL-7 treatment (Fig. 3 B). However, the levels of pSTAT5a were significantly higher (30% ± 6.5; $P < 0.002$) in T_{CM} as compared with T_{EM} (Fig. 3 C). Treatment with IL-2 also induced differential pSTAT5a levels ($P < 0.04$) between T_{CM} and T_{EM}. Indeed, 90–100% of T_{CM} showed a phosphorylated STAT5a form, compared with 50–60% observed in T_{EM}. Of note, T_{EM} present a bimodal distribution of pSTAT5a in response to IL-2, indicating that T_{EM} are heterogeneous in terms of response to IL-2.

The differences in pSTAT5a levels were not caused by differences in the levels of expression of IL-2 or IL-7 receptors. Indeed, the proportion of cells expressing CD127 (IL-7Rα), CD25 (IL-2Rα), and CD132 (γc chain) on T_{CM} were comparable to those on T_{EM} (Fig. 3 D). Of note, CD122 (IL-2Rβ) was undetectable on ex vivo T_{CM} and T_{EM} (unpublished data). Although IL-2R is expressed on ∼20% of T_{CM} as assessed by cytometry, 100% of these cells are able to phosphorylate STAT5a in response to IL-2. This suggests that T_{CM} express levels of IL-2R below the detection limits of our assay that are sufficient to induce STAT5a signaling in response to IL-2. Collectively, these results indicate that the STAT5a pathway, as shown by the levels of pSTAT5a and its downstream effectors (PIM-1 and PIM-2), is differentially regulated between T_{CM} and T_{EM}. The observed differences suggest that T_{CM} display an enhanced capacity to mobilize the STAT5a pathway for their survival as compared with T_{EM}. These results complement previous data obtained by Willinger et al., who reported that $CD8^+$ T_{CM} present a higher ability to phosphorylate STAT5a in response to both IL-2 and IL-7 than $CD8^+$ T_{EM} (31).

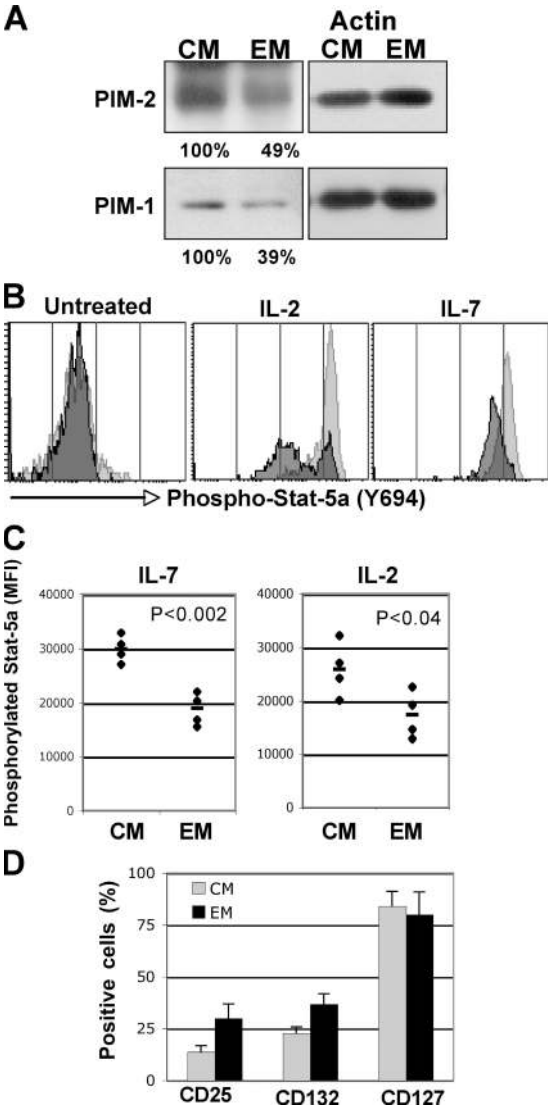

Figure 3. STAT5a signaling pathway is functionally up-regulated in T_{CM}. (A) PIM-1 and PIM-2 protein levels in ex vivo sorted T_{CM} and T_{EM} subsets. Similar results were obtained in three independent experiments. (B–D) PBMCs from healthy donors were treated with 100 U/ml IL-2 or 10 ng/ml IL-7 for 15 min at 37°C. Cells were labeled with antibodies to CD4, CD27, CCR7, CD45RA, and pSTAT5a. (B) Representative example of pSTAT5a expression levels. T_{CM}-gated cells are represented in light gray, and T_{EM}-gated cells are represented in dark gray. (C) Mean fluorescence intensity (MFI) of pSTAT5a level of expression measured in response to IL-2 or IL-7 in T_{CM} and T_{EM} ($n = 4$). Mean pSTAT5a signal values are represented by black bars. p-values (determined by the two-tailed *t* test) are shown. (D) Expression level of CD25, CD132, and CD127 in ex vivo T_{CM} and T_{EM}. PBMCs were labeled with antibodies to CD4, CD27, CCR7, and CD45RA to identify T cells subsets in conjunction with anti-CD127– or anti-CD25–specific antibodies. The results represent the proportions of CD127- and CD25-positive cells on T_{CM}- and T_{EM}-gated T cells (the percentage of positive cells ± SD of five experiments).

Regulation of the FOXO3a pathway in memory $CD4^+$ T cell subsets

FOXO3a transcriptional activity is regulated through direct phosphorylation. Once phosphorylated, FOXO3a is excluded from the nucleus and thus becomes transcriptionally inactive. FOXO3a controls the expression of several genes implicated in apoptosis and cell cycle regulation, including *FasL*, *Bim*, *Gadd45a*, *p27kip*, and *p130* (32, 33). Our gene array analysis and RT-PCR data suggested the specific involvement of the FOXO3a pathway in T_{CM} survival (Table II). Therefore, we analyzed the phosphorylation status of FOXO3a in T_{CM} and T_{EM}. We observed that the levels of pFOXO3a (S315, S253, and T32) were reproducibly ($n = 5$) more than twofold higher in ex vivo T_{CM} as compared with T_{EM}. It is worth noting that expression levels of total FOXO3a remained similar in the two memory subsets (Fig. 4 A, top). We then determined whether the observed reduction in FOXO3a phosphorylation levels seen in T_{EM} was associated with increased levels of FOXO3a target proteins. Our results show that T_{EM} expressed threefold higher levels of Bim and p130 proteins and a 1.7-fold higher expression of GADD45a when compared with the T_{CM} compartment

(Fig. 4 A, bottom). FasL, whose mRNA was clearly expressed at higher levels in T_{EM} than in T_{CM} (Table II), was undetectable in ex vivo T_{CM} and T_{EM} when assayed by Western blot and cytometry (unpublished data). However, upon T cell activation induced by PMA and ionomycine, FasL was selectively up-regulated in T_{EM} (in ~30% of the T_{EM} subset), whereas it remained undetectable in T_{CM} (Fig. 4 B). Collectively, our data show that a high expression of pFOXO3a observed in T_{CM} is associated with the shutdown of Bim, Gadd45a, and p130 proteins, thereby favoring their long-term survival.

Blocking of AKT and IκB kinase (IKK) activity prevents FOXO3a phosphorylation, leading to T_{CM} cell death

Several kinases, including AKT, IKK-β, casein kinase 1, and DYRK1A, have been reported to directly phosphorylate FOXO3a (34, 35). To identify the kinases involved in the phosphorylation of FOXO3a in T_{CM}, we analyzed FOXO3a phosphorylation in $CD4^+$ T cells ($CD4^+$ T cells were used because of the limiting amounts of T_{CM} and T_{EM} obtained after sorting) after treatment with specific kinase inhibitors. We used the pharmacological kinase inhibitors AKT-IV and wedelolactone, which inhibit AKT and IKK activities, respectively. We also tested two other kinase inhibitors: STO-609, specific for CamKK and described as an upstream mediator of AKT (36), and the MEK1/2 inhibitor U0126, used as an irrelevant kinase inhibitor. The results (Fig. 5 A) clearly showed that treatment with the AKT and IKK inhibitors led to a specific and significant reduction in the levels of pFOXO3a (S253). The expression levels of pFOXO3a (S253) in $CD4^+$ T cells were eightfold lower in the presence of the AKT inhibitor and 4.5-fold lower in the presence of the IKK inhibitor as compared with untreated cells (Fig. 5 A). It is worth noting that, in total $CD4^+$ T cells, pFOXO3a (S315) is barely detectable (unpublished data). FOXO3a can induce apoptosis through the up- regulation of proapoptotic genes (25, 34, 37, 38). To confirm the importance of the phosphorylation of FOXO3a in memory T cell survival, purified $CD4^+$ T cells were treated with different kinase inhibitors, and apoptosis was assessed using Annexin V labeling. Fig. 5 B shows that the proportion of Annexin V^+ cells is increased in a dose-dependant fashion after exposing $CD4^+$ T cells to AKT or IKK inhibitors. Moreover, we observed a significant up-regulation of the levels of the proapoptotic molecule Bim, known to be a FOXO3a target, in cells treated with AKT or IKK inhibitors (three- and eightfold, respectively; Fig. 5 C). Of note, the AKT and IKK inhibitors did not change the levels of FasL expression when assayed by Western blot or cytometry (unpublished data). These results indicated that the dephosphorylation of FOXO3a in $CD4^+$ T cells was associated with Bim up-regulation and apoptosis. None of the other kinase inhibitors tested induced apoptosis in $CD4^+$ T cells (Fig. 5 B), even when used at much higher concentrations (not depicted). Collectively, these results show that among the kinase inhibitors tested, only those able of inducing FOXO3a dephosphorylation have the capacity

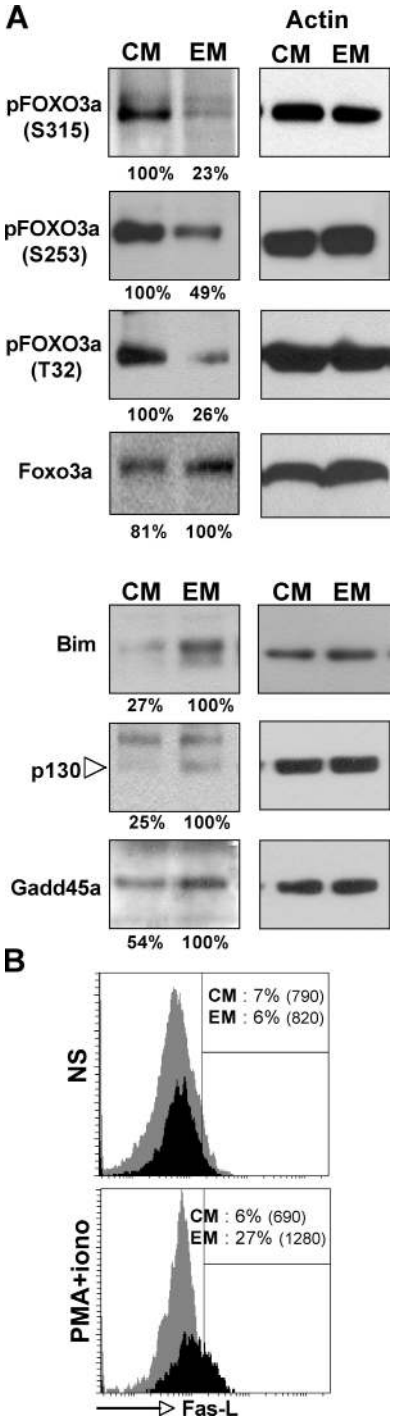

Figure 4. Regulation of the FOXO3a pathway in memory $CD4^+$ T cell subsets. (A) FOXO3a, pFOXO3a (S315, S253, or T32), Bim, p130, and Gadd45a protein levels in ex vivo sorted T_{CM} and T_{EM}. (B) Expression of FasL on activated T_{CM} (gray) and T_{EM} (black). PBMCs were activated with 10 ng/ml PMA and 500 ng/ml ionomycine for 24 h. Intracellular staining was performed using CD4, CD27, CD45RA, CCR7, and FasL antibodies. The percentages of FasL-positive cells for each subset are indicated. MFI measurements are in parentheses.

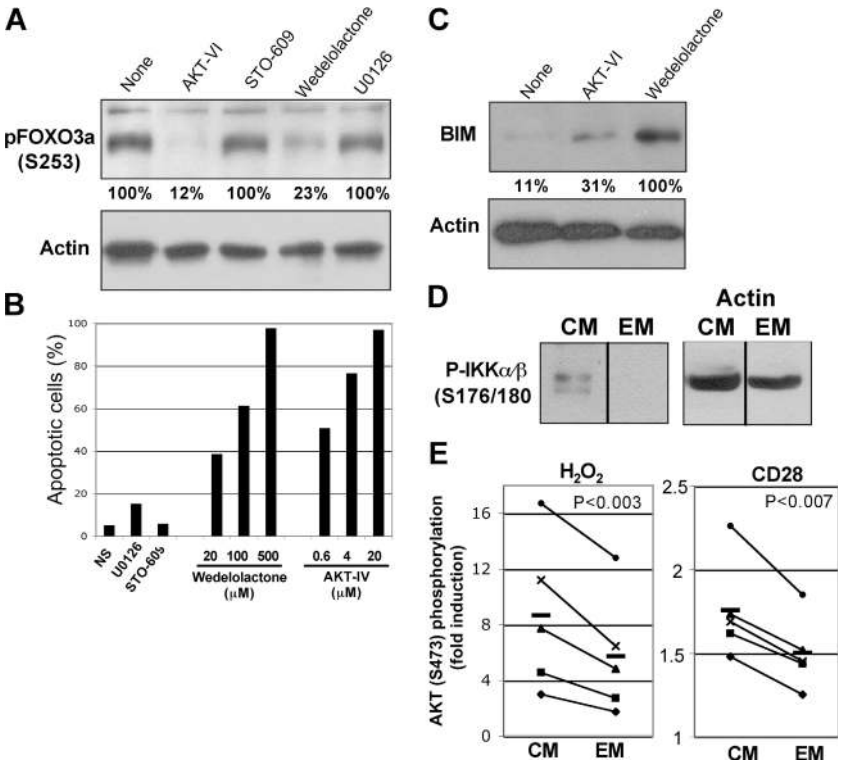

Figure 5. AKT and IKK mediate FOXO3a phosphorylation and survival in CD4 T cells. (A) Regulation of FOXO3a phosphorylation. Purified $CD4^+$ T cells were pretreated for 1 h with kinase inhibitors (10 μM AKT-VI, an AKT inhibitor; 5 μg/ml STO-609, a CamKK inhibitor; 100 μM wedelolactone, an IKK inhibitor; and 50 μM U0126, an MEK1/2 inhibitor). pFOXO3a (S253) was assessed. The results are representative of two independent experiments. (B) $CD4^+$ T cell susceptibility to apoptosis induced upon treatment with specific kinase inhibitors. $CD4^+$ T cells were cultured in the presence of kinase inhibitors for 24 h (100 μM U0126 and 10 μg/ml STO-609, and wedelolactone and AKT-IV as indicated). After 24 h, the proportion of Annexin V^+, propidium $iodide^+$ cells was quantified by flow cytometry. The results are depicted as a percentage of apoptotic cells within the total population and are representative of two independent experiments. (C) Bim expression levels in response to AKT and IKK inhibitors. $CD4^+$ T cells were treated with 1.6 μM AKT-IV or 100 μM wedelolactone for 24 h. Cells were analyzed by Western blotting using Bim specific antibodies. (D and E) Regulation of AKT and IKK phosphorylation in $CD4^+$ memory subsets. (D) pIKKαβ (S176/180) protein levels in ex vivo sorted T_{CM} and T_{EM}. Prolonged exposure did not reveal any pIKK signal in T_{EM}. Similar results were obtained in three independent experiments. (E) PBMCs from healthy donors were treated with 5 mM H_2O_2 or 2 μg/ml Ig-cross-linked CD28 for 15 min at 37°C and labeled with CD4-, CD27-, CD45RA-, and pAKT (S473)-specific antibodies. The levels of pAKT were assessed by flow cytometry in T_{CM}- and T_{EM}-gated cell subsets. The results are represented as the mean fold increase ± SD of five independent experiments, calculated as follows: (MFI of stimulated cells/MFI of unstimulated cells). p-values (determined by the two-tailed *t* test) are shown.

to induce $CD4^+$ T cell apoptosis. It is thus likely that activated AKT and IKK promote $CD4^+$ cell survival in part by phosphorylating FOXO3a, thereby repressing its transcriptional activity and leading to the down-regulation of the proapoptotic molecule Bim.

To assess the importance of AKT and IKK in the survival of memory cells, we evaluated the expression of the phosphorylated forms of these proteins in T_{CM} and T_{EM} subsets. First, pIKKα/β expression was assayed in ex vivo sorted T_{CM} and T_{EM}. Although pIKKα/β was expressed in T_{CM}, it was undetectable in T_{EM} (Fig. 5 D). Second, because the phosphorylated form of AKT was undetectable by Western blot on ex vivo sorted cells, we performed a Phosflow analysis on PBMCs treated with H_2O_2 (which is known to induce phosphorylation of AKT). The results showed that the induction of pAKT (S473) was higher in T_{CM} than T_{EM} in response to H_2O_2 (Fig. 5 E and Fig. S2, available at http://www.jem.org/cgi/content/full/jem.20061681/DC1). More importantly, in response to CD28 triggering, T_{CM} presented a modest (~20%) but consistent increase ($P < 0.007$) in AKT phosphorylation as compared with the T_{EM} (Fig. 5 E). These results suggest that in resting T_{CM}, the constitutive activation of IKKα/β could lead to FOXO3a phosphorylation. Moreover, CD28 triggering leads to higher levels of pAKT in T_{CM} and could also promote FOXO3a phosphorylation. Collectively, these results suggest that the phosphorylation levels of FOXO3a in T_{CM} can be maintained, both in their resting state and upon CD28 triggering, through the activation of IKK and AKT, respectively, thereby promoting T_{CM} survival.

The corollary of the results (Fig. 5) is that the lack of FOXO3a phosphorylation could render T_{CM} susceptible to signals inducing cell death. To determine the implication of

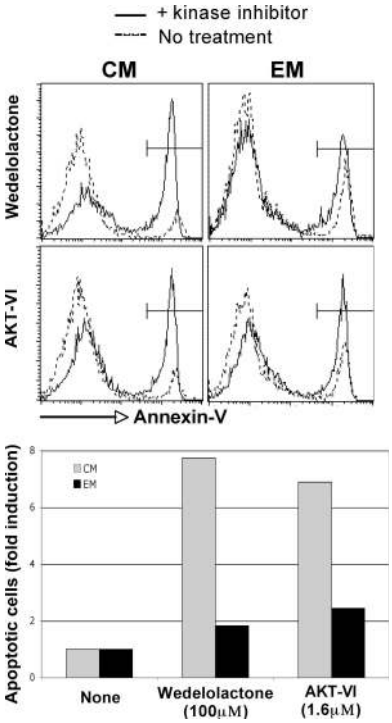

Figure 6. Susceptibility of T_{CM} and T_{EM} to apoptosis induced by kinase inhibitors. Sorted T_{CM} and T_{EM} were cultured with or without AKT and IKK inhibitors as indicated. After 24 h, the percentage of apoptotic cells was quantified by Annexin V–FITC labeling. (top) Results from a representative individual. Histogram plots show the percentage of Annexin V^+ cells in T_{CM} and T_{EM} after a 24-h exposure to AKT or IKK inhibitors. The dashed lines correspond to untreated cells, and the plain lines correspond to cells treated with kinase inhibitors. (bottom) Bar graph representation of the fold increase of apoptosis in T_{CM} and T_{EM} in response to IKK or AKT inhibitors. The fold increase of apoptosis is calculated as the percentage of apoptotic cells in treated cells divided by the percentage of apoptotic cells in untreated cells. Similar results were obtained in two independent experiments.

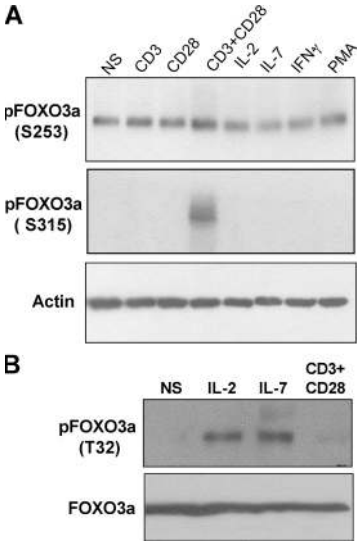

Figure 7. FOXO3a phosphorylation is dependent on TCR and cytokine engagement. (A) $CD4^+$ T cells were cultured in the presence of 2 μg/ml CD3, 2 μg/ml CD28, CD3 + CD28, 100 U/ml IL-2, 10 ng/ml IL-7, 50 μg/ml IFN-γ, or 50 ng/ml PMA for 15 min and analyzed by Western blotting for pFOXO3a (S315 and S253) expression levels. (B) $CD4^+$ T cells were cultured in the presence of 100 U/ml IL-2, 10 ng/ml IL-7, or CD3 + CD28 for 30 min and analyzed by Western blotting for pFOXO3a (T32) expression levels. The results are representative of two independent experiments.

the AKT and IKK signaling pathways in the survival of T_{CM}, we sorted T_{CM} and T_{EM} and exposed them to AKT or IKK inhibitors at their IC_{50} (1.6 μM AKT-IV and 100 μM wedelolactone). After 24 h of treatment, the proportion of apoptotic cells was quantified using Annexin V labeling (Fig. 6, top). The treatment of T_{CM} with the IKK inhibitor resulted in an eightfold increase in Annexin V^+ cells, whereas only a twofold increase was observed in T_{EM}, all relative to untreated cells ($n = 2$; Fig. 6, bottom). Similar results were also observed when these subsets were exposed to the AKT inhibitor (Fig. 6). Experiments aimed at blocking FasL triggering, using Fas-Fc chimera, in response to AKT and IKK inhibitor–induced apoptosis did not prevent T_{CM} cell death (unpublished data). These results indicate that abrogating the AKT and/or IKK survival pathways leads to apoptosis to a greater extent in T_{CM} as compared with T_{EM}, confirming that T_{CM} are primarily more dependent on these pathways for their survival. Moreover, the ability of AKT and IKK inhibitors to upregulate Bim levels of expression (Fig. 5 C) without affecting FasL expression suggests that cell death induced by these kinase inhibitors could be achieved in part through FOXO3a dephosphorylation and the subsequent increased expression of the proapoptotic molecule Bim.

TCR and cytokine triggering phosphorylate distinct sites on FOXO3a

To identify the signals that trigger FOXO3a phosphorylation in $CD4^+$ T cells, we quantified the levels of pFOXO3a (S253, S315, and T32) in response to CD3 and/or CD28 cross-linking, IL-2, IL-7, IFN-γ, and PMA treatment. pFOXO3a (S253) was easily detectable in ex vivo $CD4^+$ T cells, and none of the tested stimuli induced considerable changes in the phosphorylation status of this protein (Fig. 7 A). In contrast, FOXO3a phosphorylation on S315 was significantly induced in response to CD3 + CD28 triggering. It is worth noting that CD3 or CD28 triggering alone did not lead to FOXO3a phosphorylation (S315), indicating that the synergy of both signals is essential for FOXO3a phosphorylation at S315 (lanes 2, 3, and 4; Fig. 7 A, top). None of the other tested inducers (including γc cytokines) led to FOXO3a (S315) phosphorylation. Interestingly, the levels of pFOXO3a at T32 were drastically increased when $CD4^+$ T cells were treated with IL-7 or IL-2. No induction of pFOXO3a (T32) was observed when cells were triggered with CD3 + CD28 (Fig. 7 B). Collectively, these results indicate that TCR and γc cytokines IL-2 and IL-7 triggering induce specific FOXO3a phosphorylation at distinct sites (S315 and T32, respectively),

suggesting that the convergence of both signals is required to induce optimal FOXO3a phosphorylation and the subsequent inhibition of its transcriptional up-regulation of the proapoptotic machinery.

DISCUSSION

The involvement of TCR/ligand signaling in the generation and long-term survival of $CD4^+$ T_{CM} has been a matter of much debate. Indeed, although the persistence of both CD8 and $CD4^+$ T cells seems to occur in the absence of MHC antigen (39, 40), it has been demonstrated that repeated exposure to native or cross-reactive epitopes improves memory T cell survival and function (12, 13). Moreover, cytokines such as IL-2 and IL-7 have also been shown to enhance $CD4^+$ T_{CM} survival, although the exact mechanisms leading to this function have yet to be identified (10, 11, 41). In this paper, we focus on ex vivo polyclonal T_{CM} and T_{EM} to identify the molecular pathways involved in the maintenance and survival of memory cells. Using highly purified subsets of T_{CM} and T_{EM} obtained by multiparametric cell sorting, we propose that two converging specific signaling pathways are involved in providing T_{CM} with the capacity to survive and resist apoptotic signals. Our results indicate that TCR and γc cytokine (IL-2 and IL-7) signaling induces FOXO3a phosphorylation, thereby preventing the transcription of proapoptotic molecules such as FasL and Bim; moreover IL-2 and IL-7 allow the activation of STAT5a and the concomitant induction of several antiapoptotic molecules (PIM-1 and PIM-2). In contrast, protective functions associated with these pathways are less efficient in T_{EM} (Fig. S3, available at http://www.jem.org/cgi/content/full/jem.20061681/DC1).

In this study, we first examined the properties of T_{CM} and T_{EM}, based on a previously established classification of $CD4^+$ T cell subsets (3, 4), using transcriptional profiling by cDNA microarrays. Our results show that these two subsets exhibit considerable differences at the gene expression level, including several genes endowed with apoptotic functions. Other reports have investigated the gene expression profiles of human T_{CM} and T_{EM} in both $CD8^+$ (31, 42) and $CD4^+$ populations (43, 44). For the $CD8^+$ T cell subsets, T_{CM} clearly cluster apart from T_{EM} (31). According to the literature and our data, $CD4^+$ T_{CM} and T_{EM} also display different gene expression profiles. Despite the use of different DNA chips and different surface markers to distinguish T_{CM} ($CD45RO^+$ $CD27^+$ [44], $CD45RO^+$ $CCR7^+$ [43], or $CD45RA^-$ $CD27^+$ $CCR7^+$ in the present study) from T_{EM}, several common genes were shown to be up-regulated in T_{EM} (*ID2*, *CD63*, *CCL4*, *Grz-A*, and *DUSP6*), whereas others were up-regulated in T_{CM} (*MAL*, *CD62L*, and *CD27*) (Tables I and II; and Table S1) (43, 44). This indicates that human T_{CM} display a specific gene signature that distinguished them from T_{EM}. Among the genes differentially expressed by T_{CM} and T_{EM}, we consistently found that T_{CM} express lower levels of *Bim*, *FasL*, *Gadd45a*, and *p130*, genes that are all described as FOXO3a target genes (Tables I and II) (25–28).

FOXO3a activity is regulated through phosphorylation. In its phosphorylated form, FOXO3a is retained in the cytoplasm and is functionally inactive. Once dephosphorylated, it is translocated into the nucleus and leads to the expression of proapoptotic targeted genes such as *FasL* and *Bim* (33). Several reports have shown the role of FOXO3a-induced transcriptional activation of *FasL* or *Bim* in the active induction of apoptosis in different models. These include, for *Bim*, cytokine deprivation in lymphoid cells (38) and paclitaxel induction of apoptosis in breast cancer cells (45), and Jurkat cells and neutrophils for *FasL* (37, 46). Of note, none of those reports has investigated the synergistic role of both molecules in FOXO3a-mediated apoptosis. Using mutant forms of FOXO3a, Brunet et al. demonstrated that the localization of FOXO3a is not dependent on a specific phosphorylation site and that increased FOXO3a phosphorylation enhanced its retention in the cytosol. Higher levels of pFOXO3a lead to its increased retention in the cytoplasm (37).

Our results indicate that T_{CM} express a high level of pFOXO3a for most FOXO3a putative phospho-sites, including T32, S253, and S315. In addition, ex vivo T_{CM} present reduced levels of Bim. On the other hand, FOXO3a is significantly less phosphorylated in T_{EM}, thereby promoting its activation. Indeed, we consistently observed a significant up-regulation of FOXO3a transcriptional targets in T_{EM}: *Bim*, *p130*, and *GADD45a* at both mRNA and protein levels. The increased presence of pFOXO3a, primarily in T_{CM} (which are more resistant to apoptosis than T_{EM}), strongly suggests that elevated levels of pFOXO3a could account, in part, for this subset's resistance to Fas-mediated apoptosis and enhanced survival capacity. On the other hand, the up-regulated expression of FasL in T_{EM} upon T cell activation suggests that this subset is more sensitive to activation-induced cell death, as shown by the limited survival of these cells upon TCR triggering, as well as by their enhanced sensitivity to Fas-induced cell death (Fig. 1, D and E; and Fig. 4 B).

Several kinases appear to be involved in FOXO3a phosphorylation, including IKK and AKT (32). In this paper, we show that IKKα/β and AKT play critical roles in the phosphorylation of FOXO3a in T_{CM}. Indeed, AKT and IKK inhibitors not only prevent FOXO3a phosphorylation at S253, but also increase the expression of proapoptotic molecules such as Bim, leading to apoptosis. Moreover, we demonstrated that pIKKα/β levels are increased in T_{CM} ex vivo as compared with T_{EM}. This increased expression of activated IKK in T_{CM} could lead to FOXO3a phosphorylation and the inhibition of its transcriptional activity. Because IKK also phosphorylates IκB (a negative regulator of NF-κB), it could also result in the activation of NF-κB, the major transcription factor of several survival genes, and therefore favor T_{CM} cell survival (47). pAKT was undetectable ex vivo in both memory subsets. However, H_2O_2 or CD28 treatments lead to a more significant up-regulation of pAKT in T_{CM} as compared with T_{EM}. These results strongly suggest that T_{CM} survival ability depends, in part, upon the activation of IKK and/or AKT, whereas reduced activities of AKT and/or IKKα/β in

T_{EM} lead to the inhibition of FOXO3a phosphorylation and the subsequent induction of the proapoptotic molecule Bim. These results concur with data obtained in *Bim* knockout mice showing that the absence of Bim leads to the expansion of memory cells (48).

Our results show that the induction of FOXO3a phosphorylation at S315 required both CD3 and CD28 engagement, whereas T32 phosphorylation is dependent on γc cytokine (IL-2 and IL-7) triggering. Both AKT and IKK could be responsible for the phosphorylation of FOXO3a at S315 upon TCR/CD28 triggering. TCR signaling triggers the activation of NF-κB and IKK (49), and CD28 triggering enhances AKT phosphorylation (50). The phosphorylation of FOXO3a at T32 induced by IL-7 or IL-2 can be regulated by AKT, as Barata et al. shows that the activation of the phosphatidylinositol 3–kinase–AKT axis is mandatory for the IL-7–mediated viability of T cells (51), and IL-2 triggering can also induce AKT activation (52). Moreover, we and others also have shown that IL-4 can induce T32 phosphorylation (unpublished data) (53).

To date, no mediator has been described as a unique inducer of memory $CD4^+$ T cell survival. As such, it is possible that multiple signals with redundant or partially overlapping functions could be involved to ensure the optimal survival of memory T cells. Our results suggest that cytokines and TCR/CD3 signaling pathways converge to ensure distinct FOXO3a phosphorylation at T32 and S315, respectively. Thus, the combination of both signals could lead to higher levels of FOXO3a phosphorylated forms (quantitatively and qualitatively) and its subsequent inactivation, favoring the long-term survival of T_{CM}. Our data provide a molecular mechanism for the observation reported by Seddon et al., who demonstrated that both IL-7 and CD3 engagement are involved in maintaining homeostatic levels of T_{CM} (10). The results described here improve our understanding of the molecular mechanisms associated with T_{CM} maintenance. The identification of these mechanisms is fundamental for deciphering the dysfunction of memory cells, which is often observed in several chronic diseases, including viral infections or tumors. They also pave the way for the development of strategies aimed at restoring the functionality of these cascades through the generation of immunotherapeutics that target these pathways, thereby promoting the establishment of a long-lived memory T cell pool.

MATERIALS AND METHODS

Reagents and antibodies. Recombinant human IL-2 was obtained trough the National Institutes of Health AIDS Reagent Depository. IL-7 and IL-4 were purchased from R&D Systems. The kinase inhibitors AKT-IV, STO-069, UO126, and wedelolactone were obtained from Calbiochem. Etoposide was purchased from Sigma-Aldrich. CH11 anti-FAS agonist antibodies were obtained from Immunotech. All antibodies for flow cytometry were purchased from BD Biosciences, except for anti-CD45RA–ECD from Beckman Coulter and anti-CCR7–FITC from R&D Systems. Anti-pFOXO3a S253, anti-pFOXO3a T32, anti-pan FOXO3a, anti-Bim, anti–PIM-1, anti-pGab2 T452, anti-pIKKα/β S176/180, and anti-pAKT S473–Alexa Fluor 488 were purchased from Cell Signaling Technology, Inc.; anti-FasL (5G51) was obtained from Qbiogene; anti-P130 (clone KAB40) was purchased from Sigma-Aldrich; anti-Gadd45a was obtained from Chemicon; and anti–PIM-2 and anti-pFOXO3a S315 were gifts from BD Biosciences. Horseradish peroxidase (HRP)–conjugated goat anti–mouse and goat anti–rabbit IgG antibodies were obtained from Bio-Rad Laboratories. Anti–Rab-27a is a homemade antibody raised in rabbits against a GST-Rab-27 fusion protein.

Isolation of $CD4^+$ T cell subpopulations. PBMCs from healthy subjects (provided by J.P. Routy and R. Boulassel, McGill University, Montreal, Canada) were isolated by a Ficoll-Hypaque (GE Healthcare) density gradient. All donors signed informed consent forms approved by the Royal Victoria Hospital review board and the Centre de Recherche, CHUM. We first enriched for $CD4^+$ T cells using negative immunomagnetic bead selection (autoMACS; Miltenyi Biotec). Cells were labeled with anti-CD4–APCcy7, anti-CD45RA–ECD, anti-CD27–FITC, and anti-CCR7–PEcy7 and sorted into naive, T_{CM}, and T_{EM}. Sorting was performed using a flow cytometer (FACSAria; BD Biosciences). The purity of the T_{CM} and T_{EM} sub-populations ranged from 96 to 99%. All procedures were done at 4°C to minimize any changes in cell phenotype or gene expression.

RNA isolation, amplification, and microarray hybridization. Sample RNA was extracted using an RNA extraction kit (QIAGEN) and amplified using an RNA kit (MessageAmp; Ambion) according to the manufacturer's instructions. The amplified RNA (aRNA) was verified for quality and quantity using a bioanalyzer (model 2100; Agilent Technologies) and measuring the OD. All patient samples were hybridized against amplified universal aRNA at 37°C for 18 h on a custom human immune array. Detailed information on the labeling and hybridization procedures is available at http://www.microarrays.ca. Experimental design, sample description and preparations, hybridizations, data analysis, and annotations meet MIAME compliance.

Microarray data preprocessing. Microarrays were scanned at 16 bits using the ScanArray Express (Packard Instrument Co.). The microarrays were then screened for quality, first by visual inspection of the array with flagging of poor quality spots and then with automated scripts that scanned the quantified output files and measured overall density distribution on each channel and the number of flagged spots. Lowess normalization was then applied on the scanned chips. Microarray data is available in the National Center for Biotechnology Information Gene Expression Omnibus under accession no. GSE4741 and is titled "Convergence of TCR and cytokine signaling leads to FOXO3a phosphorylation and drives the survival of central memory $CD4^+$ T cells."

Selection of the top 100 T_{CM}/T_{EM}-discriminating genes. From the set of 19k microarray genes that passed quality control criteria during preprocessing of microarray data, we retained only the genes that significantly discriminate T_{CM} from T_{EM} according to the F-test ($P < 0.01$). From this set, a final subset of 100 genes was further manually selected according to known functions and pathways, including apoptosis, cell cycle, and signaling.

PCA. A data matrix comprising 13 T_{CM} and 13 T_{EM} samples (rows), and the 100 top T_{CM}/T_{EM}-discriminating genes (see previous section) was constructed. Using singular value decomposition of the data matrix, a standard PCA of the data's 100×100 covariance matrix was computed, with each sample comprising 100 genes. PCA was computed and plot generated by GeneLinker Platinum software (version 4.6; Improved Outcomes Software).

Two-way hierarchical clustering. Hierarchical clustering was performed over the same set of 26 samples and 100 genes as used for PCA. We used the Pearson correlation as the similarity measure between genes and samples for clustering. Analyses were performed using GeneLinker Platinum software.

Quantitative real-time PCR analysis. Changes in gene expression observed by array analyses were verified by a low density array performed on a detection system (7900 HT; Applied Biosystems). In brief, cDNA was

synthesized from total RNA (1 μg per sample) in an RT reaction in 20 μl of 1× first-strand synthesis buffer (Invitrogen). Amplification of cDNA (1:20) was performed using SYBR Green PCR buffer (PerkinElmer) containing 0.1 μM of specific primers. Before the samples were analyzed, standard curves of purified, target-specific amplicons were created. The mRNA expression for each gene was determined by comparing it with its respective standard curve. This measurement was controlled for RNA quality, quantity, and RT efficiency by normalizing it to the expression level of the *GAPDH* gene. Statistical significance was determined by use of normalized fold changes and ANOVA. The p-values were calculated using a two-tailed *t* test, assuming that the true variances were unknown.

Induction and quantification of apoptosis. Sorted cells were cultured in complete RPMI 1640 and treated as indicated in the figure legends. Apoptotic cells were detected using Annexin V labeling according to the manufacturer's protocol (Biosource International). The fluorescence signals were measured by flow cytometry using a flow cytometer (LSRI; BD Biosciences). Approximately 50,000 gated events were collected for each sample.

Western blotting analysis. T_{CM} and T_{EM} were sorted as described in Isolation of $CD4^+$ T cell subpopulations. Cells were washed twice with PBS and resuspended in lysis buffer containing 50 mM NaF and 1 mM sodium pyrophosphate. 10 μg of proteins from total cell extracts were separated on SDS-PAGE and electrotransfered onto polyvinylidene membranes (Roche). Membranes were incubated overnight at 4°C with specific antibodies, as described in the figure legends. Detection of the immune complexes was performed using HRP-conjugated goat anti–mouse (1:2,500) or goat anti–rabbit (1:3,000) IgG antibodies. HRP activity was detected using an enhanced chemiluminescence detection procedure (ECL Plus; GE Healthcare). Membranes were subsequently stripped and restained with an antiactin antibodies (1:10,000). The expression level of actin was used to control for equal loading. Protein expression levels were expressed as a percentage of the highest signals obtained.

Intracellular staining. The cells were labeled with anti-CD4–AmCyan, anti-CD27–PB, and anti-CD45RA–APCcy7 for 20 min at 4°C. The cells were fixed in 2% paraformaldehyde for 15 min at room temperature and incubated with anti–Gr-B–Alexa Fluor 700, antiperforin-FITC, or anti-FasL–PE for 20 min at room temperature in 0.5% saponin (in PBS). Analysis was performed on gated T_{CM} and T_{EM}. Approximately 20,000 gated events were collected on a flow cytometer (LSRII; BD Biosciences).

Proliferation assay. Sorted T_{CM} or T_{EM} were co-cultured with mDCs (T cell/DC ration = 40:1) in the presence of 50 ng/ml SEA. After 1–15 d of co-culture, cells were labeled with anti-CD4 and anti-TCRVβ22. For the analysis, cells were gated on $CD4^+$ T cells, and ∼150,000-gated events were collected on an LSRII flow cytometer.

Phosflow analysis of STAT5a and AKT status. PBMCs were resuspended at 20 million cells/ml in RPMI 1640 and incubated for 30 min in the presence of CCR7-FITC antibodies (20 μl/million cells) at room temperature. The cells were washed and resuspended at a cell concentration of 5 million cells/ml in PBS and stimulated for 15 min at 37°C in the presence of 100 U/ml IL-2 or 10 ng/ml IL-7. After stimulation, the cells were fixed for 10 min at 37°C using Cytofix buffer (BD Biosciences), pelleted, and permeabilized in PERM III buffer (BD Biosciences) for 30 min on ice. The cells were washed twice in staining buffer (BD Biosciences) and rehydrated for 30 min on ice in the staining buffer. Cells were labeled with anti-CD4–APCcy7, anti-CD45RA–ECD, anti-CD27–PE, and anti-pSTAT5a (Y694)–Alexa Fluor 647 specific antibodies for 30 min at room temperature. For the analysis, the cells were gated on T_{CM} and T_{EM}. An average of 20,000 gated events was collected on an LSRII flow cytometer. For CD28 cross-linking, the cells were resuspended at 10 million cells/ml in the presence of 2 μg/ml CD28 for 30 min on ice. The cells were washed twice in PBS and subsequently stimulated by cross-linking with 20 μg/ml rabbit anti–mouse Igs (Biosource International) in 25 μl of prewarmed medium for 15 min. The cells were fixed and permeabilized as described and labeled with CD4-APCcy7, CD45RA-ECD, CD27-PE, and pAKT S473–Alexa Fluor 488. Flow cytometry analysis was performed on gated T_{CM} and T_{EM}. Approximately 20,000-gated events were collected on an LSRII flow cytometer.

Online supplemental material. Table S1 shows a complete list of genes that are differentially expressed in T_{CM} and T_{EM}. Fig. S1 A shows the induction of STAT-5a phosphorylation in T_{TM}. Fig. S1 B shows real-time RT-PCR in T_{CM}, T_{EM}, and T_{TM} subsets. Fig. S2 shows histograms of Phosflow analysis of AKT phosphorylation after treatment with H_2O_2. Fig. S3 is a proposed model showing how signaling through TCR and cytokines induce survival of T_{CM}. Online supplemental material is available at http://www.jem.org/cgi/content/full/jem.20061681/DC1.

We thank Eric Massicotte for cell sorting, Marc Vendette for technical assistance, Jean-Pierre Routy and Rachid Boulassel for providing blood samples, and Abdelkader Yachou for administrative support. We also thank Nicolas Chomont, Alain Dumont, Jim Woodgett, and Sylvain Meloche for critically reviewing the manuscript.

This study was supported by funds from the National Institutes of Health, the Canadian Institutes of Health Research, Genome Quebec, Genome Canada, Fonds de Recherche en santé du Québec, and the Canadian Network for Vaccines and Immunotherapeutics. R.-P. Sekaly is the Canada Research Chair in Human Immunology.

The authors have no conflicting financial interests.

Submitted: 7 August 2006
Accepted: 29 November 2006

REFERENCES

1. Kaech, S.M., E.J. Wherry, and R. Ahmed. 2002. Effector and memory T-cell differentiation: implications for vaccine development. *Nat. Rev. Immunol.* 2:251–262.
2. Sallusto, F., J. Geginat, and A. Lanzavecchia. 2004. Central memory and effector memory T cell subsets: function, generation, and maintenance. *Annu. Rev. Immunol.* 22:745–763.
3. Sallusto, F., D. Lenig, R. Forster, M. Lipp, and A. Lanzavecchia. 1999. Two subsets of memory T lymphocytes with distinct homing potentials and effector functions. *Nature.* 401:708–712.
4. Fritsch, R.D., X. Shen, G.P. Sims, K.S. Hathcock, R.J. Hodes, and P.E. Lipsky. 2005. Stepwise differentiation of CD4 memory T cells defined by expression of CCR7 and CD27. *J. Immunol.* 175:6489–6497.
5. Wu, C.Y., J.R. Kirman, M.J. Rotte, D.F. Davey, S.P. Perfetto, E.G. Rhee, B.L. Freidag, B.J. Hill, D.C. Douek, and R.A. Seder. 2002. Distinct lineages of T(H)1 cells have differential capacities for memory cell generation in vivo. *Nat. Immunol.* 3:852–858.
6. Zaph, C., J. Uzonna, S.M. Beverley, and P. Scott. 2004. Central memory T cells mediate long-term immunity to *Leishmania major* in the absence of persistent parasites. *Nat. Med.* 10:1104–1110.
7. Letvin, N.L., J.R. Mascola, Y. Sun, D.A. Gorgone, A.P. Buzby, L. Xu, Z.Y. Yang, B. Chakrabarti, S.S. Rao, J.E. Schmitz, et al. 2006. Preserved CD4+ central memory T cells and survival in vaccinated SIV-challenged monkeys. *Science.* 312:1530–1533.
8. Sad, S., and L. Krishnan. 2003. Maintenance and attrition of T-cell memory. *Crit. Rev. Immunol.* 23:129–147.
9. Macallan, D.C., D. Wallace, Y. Zhang, C. De Lara, A.T. Worth, H. Ghattas, G.E. Griffin, P.C. Beverley, and D.F. Tough. 2004. Rapid turnover of effector–memory $CD4^+$ T cells in healthy humans. *J. Exp. Med.* 200:255–260.
10. Seddon, B., P. Tomlinson, and R. Zamoyska. 2003. Interleukin 7 and T cell receptor signals regulate homeostasis of CD4 memory cells. *Nat. Immunol.* 4:680–686.
11. Kondrack, R.M., J. Harbertson, J.T. Tan, M.E. McBreen, C.D. Surh, and L.M. Bradley. 2003. Interleukin 7 regulates the survival and generation of memory CD4 cells. *J. Exp. Med.* 198:1797–1806.
12. Patke, D.S., and D.L. Farber. 2005. Modulation of memory CD4 T cell function and survival potential by altering the strength of the recall stimulus. *J. Immunol.* 174:5433–5443.

13. Kassiotis, G., R. Zamoyska, and B. Stockinger. 2003. Involvement of avidity for major histocompatibility complex in homeostasis of naive and memory T cells. *J. Exp. Med.* 197:1007–1016.
14. Seder, R.A., and R. Ahmed. 2003. Similarities and differences in CD4+ and CD8+ effector and memory T cell generation. *Nat. Immunol.* 4:835–842.
15. Haddad, E.K., X. Wu, J.A. Hammer III, and P.A. Henkart. 2001. Defective granule exocytosis in Rab27a-deficient lymphocytes from Ashen mice. *J. Cell Biol.* 152:835–842.
16. Hitoshi, Y., J. Lorens, S.I. Kitada, J. Fisher, M. LaBarge, H.Z. Ring, U. Francke, J.C. Reed, S. Kinoshita, and G.P. Nolan. 1998. Toso, a cell surface, specific regulator of Fas-induced apoptosis in T cells. *Immunity.* 8:461–471.
17. Yan, B., M. Zemskova, S. Holder, V. Chin, A. Kraft, P.J. Koskinen, and M. Lilly. 2003. The PIM-2 kinase phosphorylates BAD on serine 112 and reverses BAD-induced cell death. *J. Biol. Chem.* 278:45358–45367.
18. Gravestein, L.A., D. Amsen, M. Boes, C.R. Calvo, A.M. Kruisbeek, and J. Borst. 1998. The TNF receptor family member CD27 signals to Jun N-terminal kinase via Traf-2. *Eur. J. Immunol.* 28:2208–2216.
19. Grossmann, M., L.A. O'Reilly, R. Gugasyan, A. Strasser, J.M. Adams, and S. Gerondakis. 2000. The anti-apoptotic activities of Rel and RelA required during B-cell maturation involve the regulation of Bcl-2 expression. *EMBO J.* 19:6351–6360.
20. Hao, Y., K. Sekine, A. Kawabata, H. Nakamura, T. Ishioka, H. Ohata, R. Katayama, C. Hashimoto, X. Zhang, T. Noda, et al. 2004. Apollon ubiquitinates SMAC and caspase-9, and has an essential cytoprotection function. *Nat. Cell Biol.* 6:849–860.
21. Hahn, H.P., M. Pang, J. He, J.D. Hernandez, R.Y. Yang, L.Y. Li, X. Wang, F.T. Liu, and L.G. Baum. 2004. Galectin-1 induces nuclear translocation of endonuclease G in caspase- and cytochrome c-independent T cell death. *Cell Death Differ.* 11:1277–1286.
22. Shannan, B., M. Seifert, K. Leskov, J. Willis, D. Boothman, W. Tilgen, and J. Reichrath. 2006. Challenge and promise: roles for clusterin in pathogenesis, progression and therapy of cancer. *Cell Death Differ.* 13:12–19.
23. Wakasugi, K., and P. Schimmel. 1999. Two distinct cytokines released from a human aminoacyl-tRNA synthetase. *Science.* 284:147–151.
24. Feng, X.H., and R. Derynck. 2005. Specificity and versatility in TGF-β signaling through Smads. *Annu. Rev. Cell Dev. Biol.* 21:659–693.
25. Essafi, A., S. Fernandez de Mattos, Y.A. Hassen, I. Soeiro, G.J. Mufti, N.S. Thomas, R.H. Medema, and E.W. Lam. 2005. Direct transcriptional regulation of Bim by FoxO3a mediates STI571-induced apoptosis in Bcr-Abl-expressing cells. *Oncogene.* 24:2317–2329.
26. Suhara, T., H.S. Kim, L.A. Kirshenbaum, and K. Walsh. 2002. Suppression of Akt signaling induces Fas ligand expression: involvement of caspase and Jun kinase activation in Akt-mediated Fas ligand regulation. *Mol. Cell. Biol.* 22:680–691.
27. Tran, H., A. Brunet, J.M. Grenier, S.R. Datta, A.J. Fornace Jr., P.S. DiStefano, L.W. Chiang, and M.E. Greenberg. 2002. DNA repair pathway stimulated by the forkhead transcription factor FOXO3a through the Gadd45 protein. *Science.* 296:530–534.
28. Kops, G.J., R.H. Medema, J. Glassford, M.A. Essers, P.F. Dijkers, P.J. Coffer, E.W. Lam, and B.M. Burgering. 2002. Control of cell cycle exit and entry by protein kinase B-regulated forkhead transcription factors. *Mol. Cell. Biol.* 22:2025–2036.
29. Morcinek, J.C., C. Weisser, E. Geissinger, M. Schartl, and C. Wellbrock. 2002. Activation of STAT5 triggers proliferation and contributes to anti-apoptotic signalling mediated by the oncogenic Xmrk kinase. *Oncogene.* 21:1668–1678.
30. Nosaka, T., T. Kawashima, K. Misawa, K. Ikuta, A.L. Mui, and T. Kitamura. 1999. STAT5 as a molecular regulator of proliferation, differentiation and apoptosis in hematopoietic cells. *EMBO J.* 18:4754–4765.
31. Willinger, T., T. Freeman, H. Hasegawa, A.J. McMichael, and M.F. Callan. 2005. Molecular signatures distinguish human central memory from effector memory CD8 T cell subsets. *J. Immunol.* 175:5895–5903.
32. Coffer, P.J., and B.M. Burgering. 2004. Forkhead-box transcription factors and their role in the immune system. *Nat. Rev. Immunol.* 4:889–899.
33. Van Der Heide, L.P., M.F. Hoekman, and M.P. Smidt. 2004. The ins and outs of FoxO shuttling: mechanisms of FoxO translocation and transcriptional regulation. *Biochem. J.* 380:297–309.
34. Medema, R.H., G.J. Kops, J.L. Bos, and B.M. Burgering. 2000. AFX-like Forkhead transcription factors mediate cell-cycle regulation by Ras and PKB through p27kip1. *Nature.* 404:782–787.
35. Hu, M.C., D.F. Lee, W. Xia, L.S. Golfman, F. Ou-Yang, J.Y. Yang, Y. Zou, S. Bao, N. Hanada, H. Saso, et al. 2004. IkappaB kinase promotes tumorigenesis through inhibition of forkhead FOXO3a. *Cell.* 117:225–237.
36. Soderling, T.R. 1999. The Ca-calmodulin-dependent protein kinase cascade. *Trends Biochem. Sci.* 24:232–236.
37. Brunet, A., A. Bonni, M.J. Zigmond, M.Z. Lin, P. Juo, L.S. Hu, M.J. Anderson, K.C. Arden, J. Blenis, and M.E. Greenberg. 1999. Akt promotes cell survival by phosphorylating and inhibiting a Forkhead transcription factor. *Cell.* 96:857–868.
38. You, H., M. Pellegrini, K. Tsuchihara, K. Yamamoto, G. Hacker, M. Erlacher, A. Villunger, and T.W. Mak. 2006. FOXO3a-dependent regulation of Puma in response to cytokine/growth factor withdrawal. *J. Exp. Med.* 203:1657–1663.
39. Murali-Krishna, K., L.L. Lau, S. Sambhara, F. Lemonnier, J. Altman, and R. Ahmed. 1999. Persistence of memory CD8 T cells in MHC class I-deficient mice. *Science.* 286:1377–1381.
40. Swain, S.L., H. Hu, and G. Huston. 1999. Class II-independent generation of CD4 memory T cells from effectors. *Science.* 286:1381–1383.
41. Dooms, H., E. Kahn, B. Knoechel, and A.K. Abbas. 2004. IL-2 induces a competitive survival advantage in T lymphocytes. *J. Immunol.* 172:5973–5979.
42. Holmes, S., M. He, T. Xu, and P.P. Lee. 2005. Memory T cells have gene expression patterns intermediate between naive and effector. *Proc. Natl. Acad. Sci. USA.* 102:5519–5523.
43. Chtanova, T., R. Newton, S.M. Liu, L. Weininger, T.R. Young, D.G. Silva, F. Bertoni, A. Rinaldi, S. Chappaz, F. Sallusto, et al. 2005. Identification of T cell-restricted genes, and signatures for different T cell responses, using a comprehensive collection of microarray datasets. *J. Immunol.* 175:7837–7847.
44. Schiott, A., M. Lindstedt, B. Johansson-Lindbom, E. Roggen, and C.A. Borrebaeck. 2004. CD27− CD4+ memory T cells define a differentiated memory population at both the functional and transcriptional levels. *Immunology.* 113:363–370.
45. Sunters, A., S. Fernandez de Mattos, M. Stahl, J.J. Brosens, G. Zoumpoulidou, C.A. Saunders, P.J. Coffer, R.H. Medema, R.C. Coombes, and E.W. Lam. 2003. FoxO3a transcriptional regulation of Bim controls apoptosis in paclitaxel-treated breast cancer cell lines. *J. Biol. Chem.* 278:49795–49805.
46. Jonsson, H., P. Allen, and S.L. Peng. 2005. Inflammatory arthritis requires Foxo3a to prevent Fas ligand-induced neutrophil apoptosis. *Nat. Med.* 11:666–671.
47. Siebenlist, U., K. Brown, and E. Claudio. 2005. Control of lymphocyte development by nuclear factor-kappaB. *Nat. Rev. Immunol.* 5:435–445.
48. Wojciechowski, S., M.B. Jordan, Y. Zhu, J. White, A.J. Zajac, and D.A. Hildeman. 2006. Bim mediates apoptosis of CD127(lo) effector T cells and limits T cell memory. *Eur. J. Immunol.* 36:1694–1706.
49. Weil, R., K. Schwamborn, A. Alcover, C. Bessia, V. Di Bartolo, and A. Israel. 2003. Induction of the NF-kappaB cascade by recruitment of the scaffold molecule NEMO to the T cell receptor. *Immunity.* 18:13–26.
50. Appleman, L.J., A.A. van Puijenbroek, K.M. Shu, L.M. Nadler, and V.A. Boussiotis. 2002. CD28 costimulation mediates down-regulation of p27kip1 and cell cycle progression by activation of the PI3K/PKB signaling pathway in primary human T cells. *J. Immunol.* 168:2729–2736.
51. Barata, J.T., A. Silva, J.G. Brandao, L.M. Nadler, A.A. Cardoso, and V.A. Boussiotis. 2004. Activation of PI3K is indispensable for interleukin 7–mediated viability, proliferation, glucose use, and growth of T cell acute lymphoblastic leukemia cells. *J. Exp. Med.* 200:659–669.
52. Kelly, E., A. Won, Y. Refaeli, and L. Van Parijs. 2002. IL-2 and related cytokines can promote T cell survival by activating AKT. *J. Immunol.* 168:597–603.
53. Bilancio, A., K. Okkenhaug, M. Camps, J.L. Emery, T. Ruckle, C. Rommel, and B. Vanhaesebroeck. 2006. Key role of the p110delta isoform of PI3K in B-cell antigen and IL-4 receptor signaling: comparative analysis of genetic and pharmacologic interference with p110delta function in B cells. *Blood.* 107:642–650.